Pergamon

Geochimica et Cosmochimica Acta, Vol. 60, No. 18, pp. 3399–3414, 1996
Copyright © 1996 Elsevier Science Ltd
Printed in the USA. All rights reserved
0016-7037/96 $15.00 + .00

PII S0016-7037(96)00169-X

Surface-charge properties and UO_2^{2+} adsorption of a subsurface smectite

G. D. TURNER, J. M. ZACHARA,* J. P. MCKINLEY, and S. C. SMITH
Pacific Northwest National Laboratory, Environmental and Energy Sciences Division, Richland, WA 99352, USA

(*Received December* 8, 1994; *accepted in revised form May* 19, 1996)

Abstract—Surface charge and UO_2^{2+} adsorption were measured on a clay-sized, subsurface mineral isolate whose mineralogy was dominated by a ferrogenous beidellite. Experiments were performed in batch at 25°C with $N_{2(g)}$ atmosphere and sorbent suspensions (9.46 g clay/kg suspension) that had been adjusted in pH between 4 and 9. Surface charge was defined by measurements of adsorbed Na by isotopic exchange and of proton adsorption by potentiometric titration in $NaClO_4$ ($I = 0.1, 0.01, 0.001$). Extraction of the clay with $La(NO_3)_3$ and aqueous-phase analyses were necessary to establish the contributions of Al and Si dissolution to the proton balance and the total adsorbed cation charge (i.e., $Na^+_{ads} + 3Al^{3+}_{ads}$). The adsorption of UO_2^{2+} (7.5×10^{-6} mol L^{-1}) was determined in Na^+ (0.1, 0.01, 0.001 mol L^{-1}) and Ca^{2+} (0.05 and 0.005 mol L^{-1}) electrolytes. Adsorption of UO_2^{2+} showed contributions of ion exchange and edge complexation reactions in Na^+ electrolyte, but by only edge complexation reactions in Ca^{2+} electrolyte. A multiple-site surface-complexation model containing fixed- (X^-) and variable-charge sites (SiOH, AlOH) was fit to adsorbed cation charge data between pH 4 and 10, with the concentrations of AlOH, SiOH, and X^- as the adjustable parameters. Surface acidity and ion-pair formation constants for gibbsite and silica were used to describe the ionization and electrolyte binding of the AlOH and SiOH sites. The model provided an excellent description of the surface-charge characteristics of the clay as measured by sodium isotopic exchange and potentiometric titration. A composite model was formulated to predict UO_2^{2+} adsorption by incorporating UO_2^{2+} aqueous speciation, competitive ion exchange with background electrolyte cations, and UO_2^{2+} complexation with AlOH and SiOH sites. UO_2^{2+} complexation with AlOH and SiOH was parameterized by UO_2^{2+} sorption on α-$Al(OH)_3(s)$ and α-$SiO_2(s)$, respectively. The composite model overpredicted UO_2^{2+} sorption across the entire pH range in both electrolytes. Acceptable predictions could be obtained if the UO_2^{2+} affinity for edge AlOH sites were adjusted 2.03 log units below that of gibbsite. Changes in chemical affinity arising from lattice substitutions and edge site morphology are, therefore, concluded to contribute significantly to adsorption, although the potential competitive effects of dissolved Al^{3+} and H_4SiO_4 could not be discounted. The adsorption of UO_2^{2+} on the subsurface smectite was similar to that of the reference montmorillonite, SWy-1, with the exception that Al dissolution contributed significantly to adsorbed cation charge.

1. INTRODUCTION

Uranium exhibits an intriguing low-temperature geochemistry. Uranium is also of fundamental importance in the nuclear fuel cycle, where it serves as a source element and results as a ubiquitous waste component. There is concern regarding the environmental geochemistry of U in oxidized subsurface systems where it has been released to groundwaters as a result of mining, milling, and disposal of tailings (Morrison and Cahn, 1991) and as a result of nuclear processing and weapons development (Riley et al., 1992).

Under oxidizing geochemical conditions, the most stable valence of U is U(VI) (Grenthe, 1992), which exists in acidic aqueous solutions as the uranyl ion, UO_2^{2+}. Uranyl hydrolyses extensively at higher pH, forming monomers, dimers, and trimers. The uranyl ion is fairly mobile in oxidizing groundwater through formation of anionic carbonate complexes, which are weakly sorbed by many mineral forms (Hsi and Langmuir, 1985; Waite et al., 1994). Sorption is widely recognized as a primary process controlling the aqueous concentration of U(VI) in groundwater (Thomson et al., 1986; Payne and Waite, 1991). Sorption to layer silicates is implicated in formation of U(IV) deposits, with sorption of U(VI) functioning as a preconcentration vector prior to reduction (Fiala, 1988; Giblin, 1980).

Smectites form through the weathering of feldspars, mica, and other phases (Borchardt, 1989), and their small size and surface properties make them important reactive components of sedimentary rocks such as shale and mudstone, as well as regolith and soils formed from such materials. These 2:1 layer silicates contain (1) fixed negative charge sites as a result of isomorphic structural substitutions and (2) ionizable hydroxyl sites exposed along the truncated tetrahedral and octahedral layers on the crystallite edge. Both fixed charge and hydroxyl sites form surface complexes with metal cations (Fletcher and Sposito, 1989; Stadler and Schindler, 1993; Zachara et al., 1993; Zachara and McKinley, 1993; Zachara and Smith, 1994). The uranyl ion is strongly sorbed by the reference smectite, SWy-1 (Tsunashima et al., 1981; Dent et al., 1992; McKinley et al., 1996). Both modeling and spectroscopic studies indicate that multiple surface species resulting from ion exchange on fixed charge sites and surface coordination reactions to edge hydroxyls are responsible for UO_2^{2+} sorption to smectite (Zachara and McKinley, 1993; Morris et al., 1994; Chisholm-Brause et al., 1994; McKinley et al., 1996). While studies of specimen solids like SWy-1 provide important insights into the geochemical behavior of smectites in subsurface systems, natural smectites may show

---

* Author to whom correspondence should be addressed.

1/110

DOCUMENT CLASSIFICATION
REVIEW WAIVER PER
CLASSIFICATION OFFICE

Best Available Copy

ADMIN RECORD
SW-A-004644

behavioral differences as a result of dissimilarities in particle size, mineralogy and chemical composition, accessory phases, and other variables (Zachara et al., 1993, Zachara and Smith, 1994).

In this communication, we investigate the sorption properties of a shale-derived smectite for UO_2^{2+} over ranges in pH and ionic strength. The effects of solubilized Al and Si on the measured surface properties of the clay and on UO_2^{2+} adsorption are considered. A multiple-site surface chemical model is developed for the subsurface smectite, based on acid-base titrations and measurements of electrolyte cation adsorption. The adsorption of UO_2^{2+} is interpreted within the context of this site-binding model and its own complex hydrolysis behavior.

2. EXPERIMENTAL PROCEDURES

2.1. Clay Isolation and Characterization

2.1.1. Clay isolation and preparation

Clay-sized material (<2 μm) dominated by smectite was isolated from a shale-derived regolith. The regolith underlies the Kenoma silt loam (fine, montmorillonitic, thermic Vertic Argiudoll) in eastern Kansas. Clay-sized fractions were separated by sedimentation from Na^+-saturated material that had been sieved to <2 mm. The clay isolate was concentrated by flocculation with $NaClO_4$ and then dialyzed against deionized water (DI-H_2O) until the dialysate conductivity was <0.5 mS cm^{-1}. The clay isolate was then extracted with dithionite-citrate-bicarbonate (DCB; Kittrick and Hope, 1963) to remove small amounts of reducible Fe oxides and associated organic matter. The extracted isolate was then treated three times with 3% H_2O_2 to oxidize residual reductant, organic matter, and sorbed citrate. Such treatment readily oxidizes any structural Fe(II) that may have been reduced by DCB treatment (Lear and Stucki, 1989; Komadel et al., 1990). The extracted isolate was then dialyzed against DI-H_2O and freeze-dried. The <2-μm fraction of a Wyoming montmorillonite, SWy-1, from the Clay Minerals Society was prepared identically (McKinley et al., 1996) for comparative purposes during characterization.

2.1.2. Surface area, mineralogy, and reactive sites

External surface area was measured by multipoint $N_{2(g)}$ adsorption, and total surface area was measured by ethylene glycol monoethyl ether adsorption (EGME; Chihacek and Bremner, 1979). The mineralogy of the Kenoma clay isolate was characterized by X-ray diffraction (XRD), using the ion saturation and heat treatments proposed by Harward et al. (1969) and by chemical analysis as reported in Zachara et al. (1993).

Fixed and pH variable surface charge was measured at pH 6 using Cs^+ saturation (Anderson and Sposito, 1991). The clay isolate (0.225 g) was equilibrated with CsCl (0.05 mol L^{-1}) at pH 6, and washed with ethanol. The Cs^+-saturated clay was then dried at 65°C to promote dehydration of the Cs^+ cation and reaction with the ditrigonal cavities of the smectite. Following drying, the clay isolate was extracted with 0.01 mol L^{-1} LiCl to displace the Cs^+ from ionized edge sites (SO^-). Finally, the clay isolate was extracted exhaustively with 1 mol L^{-1} ammonium acetate to displace Cs^+ from the ditrigonal cavities (fixed-charge sites, X^-). The extracts were analyzed for Cs^+ by inductively coupled argon plasma spectroscopy (ICP), and mass concentrations of X^- and SO^- sites were computed accordingly.

The total concentration of hydroxylated surface sites was measured by ^3H exchange (Yates, 1975). The clay isolate was prepared for ^3H exchange by washing three times in 0.5 mol L^{-1} $CsClO_4$, followed by dialysis against DI-H_2O and freeze-drying. The clay isolate was equilibrated with a solution of tritiated, DI-H_2O for 16 h. Following equilibration, the tritiated solids were frozen with $N_{2(l)}$, and the suspensions were sublimed at 10^{-4} Pa for 24 h to remove physically adsorbed water. After sublimation, the tritiated clay isolates were resuspended in DI-H_2O and replicate pairs of samples were allowed to equilibrate for 15 min, 1 h, and 4 h. Finally, a sample of the supernatant was evaluated for ^3H activity after each of the equilibration periods. Tritium activity was evaluated by liquid scintillation analysis on a Packard 2500TR liquid-scintillation counter. As a quality control measure, goethite was prepared and analyzed identically to the clay isolate.

2.2. Proton and Electrolyte Cation Adsorption

2.2.1. Reagents

Acid titrants (0.1 and 0.01 mol L^{-1} HCl) were prepared from Baker Ultrex II reagent-grade HCl by dilution in DI-H_2O. Basic titrants (0.1 and 0.01 mol L^{-1} NaOH) were prepared from Baker CO_2-free, reagent-grade Dilute-It® ampules by dilution in DI-H_2O under a $N_{2(g)}$ atmosphere. The 0.1 mol L^{-1} HCl titrants were standardized against 0.10 g of Fisher ACS primary standard reagent-grade Tris (hydroxymethyl) aminomethane; 0.1 mol L^{-1} NaOH titrants were standardized against 0.15 g of Aldrich ACS primary standard potassium hydrogen phthalate using a Mettler DL40 programmable titrator under a $N_{2(g)}$ atmosphere. Subsequently, the 0.01 mol L^{-1} titrants were standardized against the 0.1 mol L^{-1} titrants. Both the accuracy and the precision of the standardization procedure were within 0.0002 mol L^{-1}. Electrolyte solutions were prepared from reagent-grade chemicals with degassed DI-H_2O under a $N_{2(g)}$ atmosphere. Degassed DI-H_2O was prepared in a 4 L Pyrex® flask by bringing to a boil under vacuum, followed by cooling under an $N_{2(g)}$ atmosphere.

2.2.2. Adsorbed cation charge

Adsorbed Na (Na_{ads}; mol kg^{-1} of clay) was determined by isotopic dilution using a modification of the procedure of Babcock and Schultz (1970). Reagents and suspensions were prepared with degassed DI-H_2O, and experiments were performed under an $N_{2(g)}$ atmosphere at 25°C. The degassed DI-H_2O and $N_{2(g)}$ atmosphere were employed to minimize contamination from atmospheric $CO_{2(g)}$ and the subsequent effect of aqueous carbonate speciation on the solution proton balance. Adsorbed Na^+ was measured with a solids concentration of 9.49 g clay kg^{-1} solvent in 0.01 and 0.001 mol kg^{-1} ^{22}Na-NaCl electrolyte solutions between pH 4 and 10. Stock suspensions of the freeze-dried clay were prepared at 11.2 g clay kg^{-1} of solvent in 0.012 and 0.0012 mol kg^{-1} NaCl and allowed to rehydrate for 24 h. Following equilibration, 17 mL of the stock suspensions were transferred to tared 50-mL polycarbonate centrifuge tubes. Predetermined volumes of either HCl or NaOH titrants were then combined by mass with DI-H_2O in 4-mL polystyrene tubes to yield a total titrant spike volume of 1 mL, which was then transferred to the clay suspensions by mass. Next, 2 mL of a $^{22}Na^+$-labelled stock solution containing 100,000 dpm g^{-1} ^{22}Na-NaCl were transferred to the pH-adjusted suspensions by mass. The pH-adjusted, $^{22}Na^+$-spiked suspensions were then equilibrated for 24 h with mild agitation under $N_{2(g)}$. Following equilibration, the suspensions were centrifuged at 26,895 rcf for 30 min, and two 0.5-mL samples of supernatant were removed for liquid-scintillation analysis of $^{22}Na^+_{(aq)}$. One 4-mL sample of supernatant was removed for analysis of total $Na^+_{(aq)}$ by ion chromatography. The supernatant pH was determined using a Microelectrodes MI-410 microcombination pH electrode calibrated against standard buffer solutions.

2.2.3. Potentiometric, titration, and Al/Si dissolution

Proton adsorption, mineral phase dissolution, and exchangeable cations (Na^+, Al^{3+}) were determined simultaneously by a discontinuous batch titration procedure identical to that used for the Na_{ads} determination. The titration was followed by an extraction with 0.01 mol L^{-1} $La(NO_3)_3$ to displace exchangeable cations. Final suspensions contained 9.49 g clay kg^{-1} solution in 0.01 and 0.001 mol kg^{-1} NaCl over the pH range 4–10. Following a 24 h equilibration, the suspensions were centrifuged at 26,895 rcf for 30 min. Two 5-mL samples of supernatant were filtered through pretreated Amicon CF25 Centriflo membrane cones having a mean pore diameter of 1.8 nm. The filtrate was acidified to 5% HCl by mass and retained for analysis of aqueous cations by inductively coupled argon plasma

2

Table 1. Properties of the DCB-H_2O_2 Treated Kenoma Clay[a]

Mean Particle Diameter[b] (µm)	Surface Area ($m^2\ g^{-1}$) N_2	EGME	CEC[c] @ pH 6	$[SO^-]$[d]	$[X^-]$[d]	$[SOH]_T$[e]	$[SOH]_T$[f]
			x 10^{-2} mol kg^{-1}				
0.16 ± 0.12	99	348	45.4	15.1	34.8	86.1	11.7

[a] chemical formula determined by chemical analysis (Zachara et al., 1993): $(Ca_{0.01}Na_{0.47}K_{0.31})(Al_{2.99}Fe(III)_{0.545}Mg_{0.277}Ti_{0.08})(Si_{7.74}Al_{0.26})O_{20}(OH)_2$

[b] mean particle diameter determined by TEM (Zachara et al., 1993)

[c] CEC = $Na_{(ads)}$ at pH 6 as determined by isotopic exchange with $^{22}Na^+$

[d] $[SO^-]$ = Li^+ displaceable Cs^+, $[X^-]$ = NH_4^+ displaceable Cs^+ (Anderson and Sposito, 1991). The total of these represents an alternative measure of CEC at pH 6.

[e] by tritium exchange

[f] computed from particle size and crystallographic data (Zachara and Smith, 1994)

mass spectrometry (ICP–MS). Following pH determination and a second centrifugation, the remaining supernatant was discarded, and the occluded mass was determined. The clay isolate pellets were resuspended in 10 mL 0.01 mol L^{-1} $La(NO_3)_3$. The suspensions were immediately centrifuged, and the supernatant was collected into tared 30-mL polyethylene bottles. The clay pellets were treated twice more with 10 mL 0.01 mol L^{-1} $La(NO_3)_3$. The total mass of the $La(NO_3)_3$ extract was determined, and subsamples were filtered, acidified, and retained for ICP-MS analysis as before. Pretreatment of the CF25 membrane cones consisted of soaking in DI-H_2O at pH 2, rinsing with two 7-mL volumes of fresh DI-H_2O, and rinsing with one 7-mL waste volume of supernatant or extract filtrate prior to collecting the final sample for analysis.

2.3. Uranyl Adsorption

Adsorption of UO_2^{2+} (8.4×10^{-6} mol L^{-1}) was determined using a pH-stat technique followed by extraction with 0.01 mol L^{-1} $La(NO_3)_3$ to quantify exchangeable Al^{3+}. The experiments used a suspension concentration of 1.5 g clay kg^{-1} of solvent in three concentrations of $NaClO_4$ (0.001, 0.01, and 0.1 mol L^{-1}) and two concentrations of $Ca(ClO_4)_2$ (0.005 and 0.05 mol L^{-1}). Reagents and suspensions were prepared with degassed DI-H_2O, and experiments were performed under an $N_{2(g)}$ atmosphere at 25°C. The degassed DI-H_2O and $N_{2(g)}$ atmosphere were employed to minimize contamination from atmospheric $CO_{2(g)}$ and the subsequent uranyl-carbonate speciation. Aqueous carbonate ligands compete effectively with sorption sites for free UO_2^{2+} (Hsi and Langmuir, 1985; Lieser and Thybusch, 1988; Lieser et al., 1992). Perchlorate was used as the electrolyte anion to minimize metal-ligand complexation (Fletcher and Sposito, 1989). Suspensions were prepared at the desired sorbent and electrolyte concentrations in 500-mL jacketed reaction vessels. The suspension was allowed to equilibrate and rehydrate at pH 4 for 12 h using a Radiometer autotitrator in pH stat mode with a titrant of 0.1 mol L^{-1} $HClO_4$. pH was monitored with the cell:

$$Hg/Hg_2Cl_2/KCl_{sat'd}//NaClO_4 \text{ agar } (0.001, 0.01, \text{ or } 0.1 \text{ mol } L^{-1})/$$
$$/\text{suspension/glass/}HCl\ (0.1 \text{ mol } L^{-1})/AgCl/Ag.$$

An agar bridge containing electrolyte at the appropriate concentration was used to prevent contamination from the KCl filling solution in the reference electrode.

Following equilibration, the suspension was spiked with 5 mL of a 8.4×10^{-4} mol L^{-1} UO_2^{2+} stock solution prepared from uranyl nitrate ($UO_2(NO_3)_2 \cdot 6H_2O$; >99.0% purity; Fluka Chemicals). pH was adjusted upward with 0.1 mol L^{-1} NaOH in 0.5-pH increments, to span a range of 4–9. At each pH, duplicate 25-mL samples of the suspension were removed to 50-mL polycarbonate centrifuge tubes. The pH-adjusted samples were equilibrated for 24 h with mild agitation under $N_{2(g)}$. Following equilibration, the samples were centrifuged at 26,895 rcf for 30 min. Two 5-mL samples of supernatant were filtered through pretreated Amicon CF25 Centriflo Membrane Cones, acidified to 5% HCl, and retained for ICP–MS analysis of Al, Na, Ca, and Si as before. One 4-mL sample of supernatant was analyzed for U with a kinetic phosphorescence analyzer (CHEMCHEK Inst., Inc. Model KPA-11). The detection limit and analytical precision of the analyses were 1.11×10^{-9} mol L^{-1} and 3.33×10^{-10} mol L^{-1}, respectively. The final pH of the supernatant was measured. Following pH determination, the suspensions were again centrifuged, and the remaining supernatant was discarded. The mass of the occluded volume was determined, and the pellets were resuspended in 10 mL 0.01 mol L^{-1} $La(NO_3)_3$ solutions pH-adjusted to match the final supernatant pH. The suspensions were again centrifuged, and two 5-mL aliquots of the supernatant were filtered, acidified, and retained for ICP–MS analysis as before.

3. RESULTS

3.1. Solid Phase Properties

Chemical analysis and XRD have previously indicated that ferrogenous beidellite, mica, and fine grained quartz are the principle mineralogic components of the clay isolate (Zachara et al., 1993). The comparative properties of this subsurface smectite to SWy-1 (Source Clays Repository) have also been reported (Zachara et al., 1993; Zachara and McKinley, 1993; Zachara and Smith, 1994). The Kenoma smectite is of smaller particle size and exhibits a lower CEC than SWy-1. As a result of its smaller particle size, the Kenoma smectite has a larger $N_{2(g)}$ surface area than does SWy-1. Selected properties of the Kenoma smectite are summarized in Table 1.

The cation exchange capacities of the subsurface smectite at pH 6 were measured by Na adsorption (0.454 mol kg^{-1}) and Cs saturation ($[SO^-] + [X^-] = 0.498$ mol kg^{-1}) (Table 1). The Anderson and Sposito (1991) procedure indicated that as much as 30% of the Cs-CEC at pH 6 ($[SO^-] = 0.15$ mol kg^{-1}) might originate from hydroxyl site ionization (Table 1). The total concentration of surface hydroxyls measured by ^3H exchange (Table 1) was 7.4 times that estimated

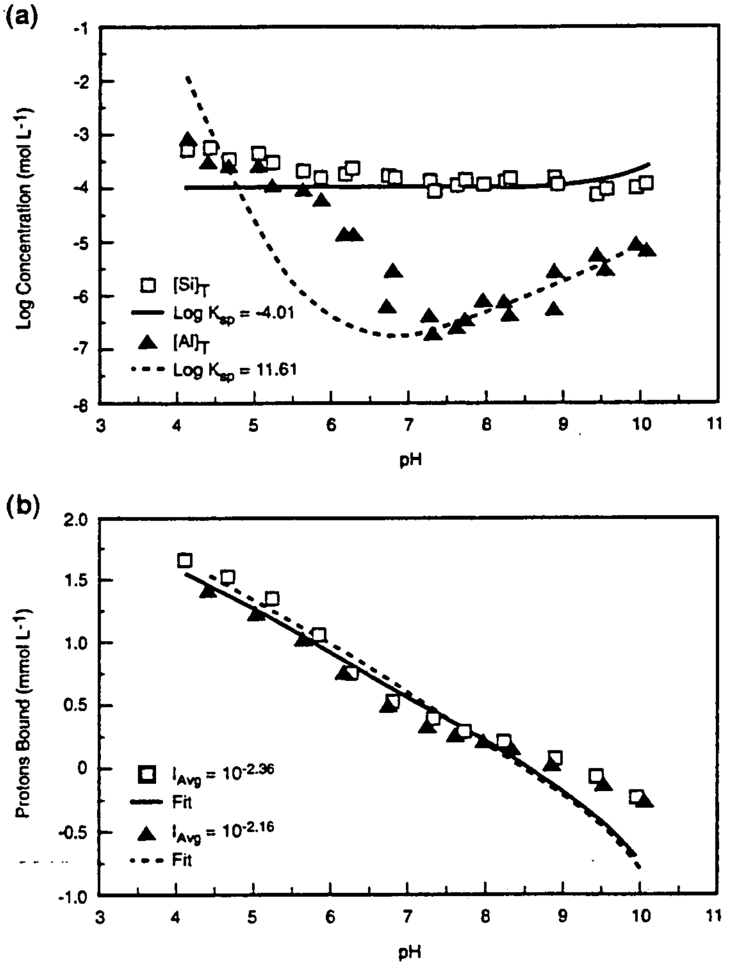

FIG. 1. (a) Concentrations of $[\mathrm{Al}]_T$ and $[\mathrm{Si}]_T$ measured in the potentiometric titration experiments. Best-fit solubility products are illustrated for $[\mathrm{Al}]_T$ with a dashed line, and for $[\mathrm{Si}]_T$ with a solid line. The solubility product of the gibbsite-like phase corresponds to the reaction $\mathrm{Al(OH)_{3.35}(s)} + 3.35\mathrm{H}^+ = \mathrm{Al}^{3+} + 3.35\mathrm{H_2O}$ and for the silica-like phase corresponds to the reaction $\mathrm{SiO_2(s)} + 2\mathrm{H_2O} = \mathrm{H_4SiO_4}$. (b) Concentration of protons bound by the surface and corrected for solid phase dissolution. Lines are computed using site concentrations optimized on the Na^+ material balance (Eqn. 16, Fig. 2b).

from particle size and crystallographic considerations, indicating possible contributions from surface coatings or other oxide phases such as $\mathrm{SiO}_{2(c)}$, or the effects of surface irregularities.

3.2. Proton and Electrolyte Cation Adsorption

3.2.1. Potentiometric titration

The net proton balance of a potentiometric titration may be influenced by adsorption/desorption to/from surface hydroxyls and by solid-phase dissolution and cation hydrolysis (Parker et al., 1979). Aluminum and Si concentrations were measured during titration (Fig. 1a) to quantify the impacts of dissolution on the proton balance ($\mathrm{TOT_H}$). These are reported as total concentrations, $[\ \ ]_T$, representing the sum of the aqueous and $\mathrm{La(NO_3)_3}$ extractable concentrations. Silica concentrations, $[\mathrm{Si}]_T$, were dominated by aqueous $\mathrm{H_4SiO_4}$, $[\mathrm{Si}]_{(aq)}$, and ranged between 0.1 and 1 mmol L^{-1}. The $[\mathrm{Al}]_T$ concentrations showed more pH dependence than $[\mathrm{Si}]_T$ (Fig. 1a). Below pH 7, $[\mathrm{Al}]_T$ was dominated by La^{3+}-extractable Al^{3+}; $[\mathrm{Al}]_{(aq)}$ was below analytical detection. Significant exchangeable Al^{3+} [$>10^{-4}$ mol L^{-1}] was observed up to a pH of approximately 6. The total amount of H^+ in the titrant consumed by dissolution ranged from 30% at pH 4 to 1% at pH 6. These values were high enough to complicate quantitative analysis of the proton adsorption data below pH 6.

Extractable Al^{3+} increased as the solution ionic strength decreased, indicating that ion exchange reactions on fixed-charge sites (X^-),

$$(3-n)\mathrm{Na}X + \mathrm{Al}^{3+} + n\mathrm{H_2O}$$

$$= \mathrm{Al(OH)}_n X_{(3-n)} + n\mathrm{H}^+ + (3-n)\mathrm{Na}^+ \quad (1)$$

drove the dissolution of the clay by surface complex formation. The occurrence of Al^{3+} ion exchange on montmorillonite has been previously inferred by observations of reduced Al^{3+} sorption that occur at lower pH when electrolyte concentrations are increased (Charlet et al., 1993). Neutral and anionic aqueous hydrolysis species of Al^{3+}, $[Al]_{(aq)}$, dominated $[Al]_T$ above pH 7 (Fig. 1a).

The dissolution of smectites is not well understood, and the solid phase that controls $Al^{3+}_{(aq)}$ activity has not been unambiguously identified (May et al., 1986). We fit a gibbsite-like solubility product (K_{sp}) to the $[Al]_T$ data by constraining the fit to pH > 7 (Fig. 1a). The best-fit K_{sp} exhibited a 1:3.35 Al:H stoichiometry (i.e., $Al(OH)_{3.35}$). This Al:H stoichiometry was used to correct the titration data for dissolution. Nondetectable $[Al]_{(aq)}$ concentrations below pH 7 indicated that solubility equilibrium with the aluminous phase was not achieved over the time frame of the experiments. The shape and apparent K_{sp} of the $[Si]_T$ data are more consistent with that expected for silica phases ($10^{-2.74}$ to $10^{-4.00}$; Lindsay, 1979; Williams et al., 1985) than that for smectite.

Interpretation of the potentiometric titration data (Fig. 1b) is complicated by solid phase dissolution, the unknown initial condition of the surface, and the multiplicity of proton consuming/releasing reactions (e.g., Schindler et al., 1987; Stadler and Schindler, 1993; Wanner et al., 1994). Proton adsorption (Γ_{H^+}, in mol L^{-1}) was defined as:

$$\Gamma_{H^+}\ (\text{mol L}^{-1}) = [C_A + (10^{-pH/\gamma^+})] - [C_B - (10^{-(14-pH)/\gamma^-})] - 3.35[Al]_T, \quad (2)$$

where C_A is the total concentration of H^+ added as HCl, C_B is the total concentration of OH^- added as NaOH, γ is the single ion activity coefficient computed with the Davies equation, and $[Al]_T$ is the total solubilized Al^{3+} (aqueous plus adsorbed). Our proton adsorption curves are similar in shape to those reported for bentonite by Wanner et al. (1994), although our total measured proton adsorption was markedly higher, 1.0×10^{-4} mol g^{-1} at pH 5 in this study as compared to approximately 2.0×10^{-5} mol g^{-1} (with Na = 0.05 mol L^{-1} at pH 5) reported by Wanner et al. (1994). This fivefold difference in proton adsorption density compares to a threefold difference in measured $N_{2(g)}$ surface areas: 99 m^2 g^{-1} for the Kenoma isolate and 31.5 m^2 g^{-1} for the bentonite.

The effect of $[Na]_T$ on the edge site ionization of the smectite could not be clearly discerned from the titration data because Na^+ released by the Na-saturated clay suppressed our intended hundredfold range in ionic strength. The slight enhancement in proton adsorption of the low [Na] titration over the high [Na] titration below pH 5.5 may possibly be equated to ion exchange of H^+ on fixed charge sites (Wanner et al., 1994). We surmise, however, that the effects of such exchange should be indiscernible as the reported homovalent exchange constant of H^+ for Na^+ is quite low (1.26; Fletcher and Sposito, 1989).

The pH of zero net proton adsorption in the two titrations occurred uniformly at approximately pH = 8.5 (Fig. 1b). This pH represents the resting pH of the prepared Kenoma smectite suspension, and should not necessarily be construed as the pH of zero net proton charge of the solid surface (pH_{ZNPC}; Sposito, 1984). While the pH_{ZNPC} may be close to this pH value, the resting pH is controlled by various reactions (including surface complexation and dissolution of the primary and ancillary solid phases in the isolate), and possibly particle size effects, whose contribuitons are quantitatively indeterminate in these experiments. Equally indeterminate in our procedure was the initial total hydrogen concentration (see Westall et al., 1995, for significance). The resting pH of bentonite suspensions prepared similarly occurred at approximately pH = 7.0 (Wanner et al., 1994). Stadler and Schindler (1993) reported a pH_{ZNPC} for SWy-1 prepared under acidic conditions of 7.7.

3.2.2. *Adsorbed Na and the CEC*

Adsorbed Na (Na_{ads}) showed strong pH dependence (Fig. 2a), and was weakly affected by changes in ionic strength. Below pH 6, variations in Na_{ads} with ionic strength resulted from the variable effects of $[Na]_T$ on solid-phase dissolution and surface-bound Al^{3+} (discussed previously). Exchangeable Al^{3+} was primarily responsible for the decrease in Na_{ads} below pH 6 (Fig. 2a). The total adsorbed cation charge or CEC was defined as the sum of adsorbed/exchangeable metal charge (mol_c kg^{-1}) of both Na^+ and Al^{3+}:

$$\text{CEC}\ (\text{mol}_c\ \text{kg}^{-1}) = [Na_{ads}\ (\text{mol L}^{-1}) + 3Al_{ads}\ (\text{mol L}^{-1})]/\text{clay mass (kg L}^{-1}). \quad (3)$$

The weak pH dependence of the CEC above pH 6 (Fig. 2a) resulted from the ionization of hydroxylated edge sites on the layer silicates and SiOH on the surface of silica or quartz present in the isolate. As a basis for the modeling, the CEC was redefined in terms of plausible surface complexes and counter ions contributing to the adsorbed metal charge:

$$Na_{ads} = [NaX] + [SiO^- {-} Na^+] + [AlO^- {-} Na^+] + [SiO^- {-} Na^+] + [AlO^- {-} Na^+]; \quad (4)$$

$$Al_{ads} = Al(OH)_n X_{(3-n)},^{\dagger} \quad (5)$$

where NaX and $Al(OH)_nX_{(3-n)}$ are ion-exchange complexes on fixed-charge sites (X^-), $SiO^-{-}Na^+$, and $AlO^-{-}Na^+$ are outersphere surface complexes, defined by the triple-layer model (TLM; Davis et al., 1978) and $SiO^-{-}Na^+$ and $AlO^-{-}Na^+$ represent Na retained in the diffuse layer as counter ions.

3.3. Uranyl Adsorption

The adsorption of UO_2^{2+} on the Kenoma smectite varied with pH in both $NaClO_4$ and $Ca(ClO_4)_2$ electrolytes (Fig. 3). Pronounced ionic strength effects, however, were observed only in Na electrolyte (Fig. 3a). The complex sorption behavior resulted from the pH-variable aqueous speciation of UO_2^{2+} (Fig. 4), and the sorptive contributions of fixed charge and edge hydroxyl sites with contrasting sensitivity to competition from electrolyte cations (Schindler et al., 1987; Stadler and Schindler, 1993; Zachara et al., 1993; Charlet et al., 1993; McKinley et al., 1996). The effects of aqueous speciation, especially the transition of UO_2^{2+} to lower-charged hydrolyzed species, were particularly important (McKinley et al., 1996), because the divalent cation

---

[†] In practice, this term reduces to AlX_3 because of the large exchange preference of the trivalent ion over the lower-valence hydrolyzed species. This point will be verified later in the paper.

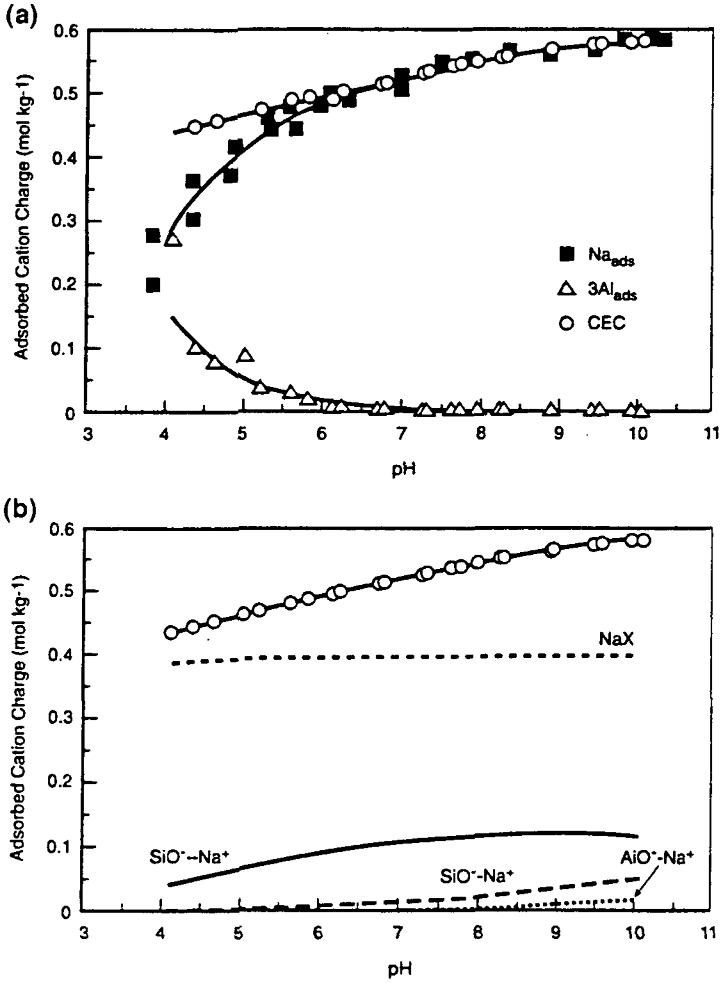

FIG. 2. (a) Adsorbed cation charge measured by isotopic dilution (Na^+) and La^{3+} displacement (Al^{3+}). The CEC is computed as the sum of these charges. Solid lines are polynomial approximations of the data used to compute the CEC. (b) Calibration of the multiple-site, surface-charge model using the adsorbed cation charge data from (a). The CEC was assumed to be homoionic and Na^+ saturated to simplify computation. Surface species are illustrated with dashed lines, and the model total is illustrated with a solid line.

is preferred on fixed-charge sites for electrostatic reasons. The decrease in adsorption with increasing ionic strength below pH 6 was consistent with suppression of the UO_2X_2 ion exchange complex (McKinley et al., 1996) through competition with Na^+ and Ca^{2+}:

$$UO_2X_2 + 2Na^+ = 2NaX + UO_2^{2+}; \quad (6)$$

$$UO_2X_2 + Ca^{2+} = CaX_2 + UO_2^{2+}. \quad (7)$$

Metal cations form strong surface complexes with hydroxylated metal cation centers on a variety of mineral surfaces (Davis and Leckie, 1978; Davis and Kent, 1990). The increase in adsorption of UO_2^{2+} from low to high pH at high ionic strength (Fig. 3) was consistent with the oxide-like surface-complexation behavior of aluminol and silanol sites at the edge of smectite (Zachara and McKinley, 1993; Zachara and Smith, 1994; McKinley et al., 1996). The observation that UO_2^{2+} reaches a maximum in adsorption at or below the pH_{ZNPC} of Al-oxide (Fig. 5a), and Fe and Ti oxides (Hsi and Langmuir, 1985; Lieser and Thybusch, 1988; Waite et al., 1994) and the lack of, or small ionic-strength dependence of UO_2^{2+} adsorption on both gibbsite and silica (Fig. 5) indicates that uranyl adsorption to edge hydroxyls involved the formation of a strong complex, possibly one that was innersphere.

4. MODELING AND DISCUSSION

The adsorption of UO_2^{2+} and its hydrolysis products was interpreted with a multiple site-binding model containing fixed charge and edge aluminol and silanol sites. Our objective in modeling was to establish a series of reactions, equilibrium constants, and site concentrations that were consistent with the surface charge measurements and that described the adsorption data. Insights were desired on the dominant sorbing species and the impacts of dissolution products from the smectite. Calculations for the surface hydroxyl sites (SiOH, AlOH) were performed with the triple-layer model (TLM; Davis et al., 1978). The reactivities of the AlOH and SiOH edge sites were represented by

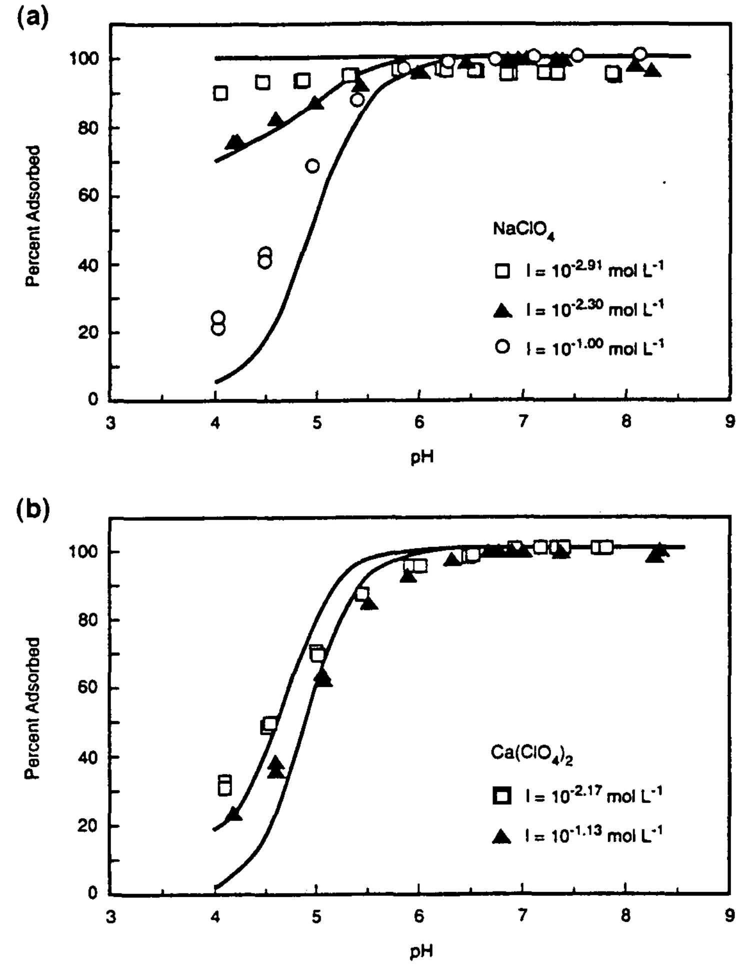

FIG. 3. Percent sorption of 8.5×10^{-6} mol L^{-1} UO$_{2(aq)}^{2+}$ in 1.5 g L^{-1} DCB/H$_2$O$_2$ treated Kenoma smectite in a) NaClO$_4$ and b) CaClO$_4$ background electrolyte. Lines illustrate model computed adsorption.

complexation constants for single phase analogues, gibbsite and silica (Table 2), respectively. Ion exchange constants describing cation adsorption on fixed charge sites were computed by the method of Fletcher and Sposito (1989), in which the exchanger phase is treated as one mole of an idealized component (X^-) having unit charge and unit activity coefficient. A similar approach was used by Stadler and Schindler (1993). The model was conceptually equivalent to treating the natural smectite material as an ideal mixture of analogue components. All multiple-site calculations were performed with the computer program FITEQL (Westall, 1982a,b).

4.1. Definition of Components

Ion exchange reactions of solutes A and B with generalized fixed-charge sites (X^-) representing one charge equivalent were described as

$$z_b A_{(aq)} + z_a BX_{z_b} = z_a B_{(aq)} + z_b AX_{z_a}, \quad (8)$$

where z_i is the valence of cation i (either A or B). Equilibrium constants, K_{AX}, for half reactions of the form

$$A^{z_a+}_{(aq)} + z_a X^- = AX_{z_a} \qquad K_{AX} \quad (9)$$

were calculated using the equation of Fletcher and Sposito (1989):

$$K_{AX} = [K_{eq}(K_{BX})^{z_a}(f_A z_b / f_B z_a) Q (z_b - z_a)]^{1/z_b}, \quad (10)$$

where K_{eq} is the equilibrium exchange constant for reaction 8, K_{BX} is the half-reaction exchange constant for an index cation—B, f_A, and f_B are surface activity coefficients for cations A and B, and Q is the compositional dependence, which is defined as the sum of the molalities, [ ], of all surface exchange complexes, AX_{z_a} and BX_{z_b}:

$$Q = ([AX_{z_a}] + [BX_{z_b}]). \quad (11)$$

Neither K_{AX} or K_{BX} is known; however, if the value of K_{BX} is arbitrarily fixed, a value of K_{AX} may be calculated to maintain consistency with K_{eq} (using Eqn. 10). For this model, the value of K_{BX} (10^{10}; Fletcher and Sposito, 1989) was chosen such that the free concentration of X^- was negligibly small, and represented the reaction:

$$Na^+_{(aq)} + X^- = NaX. \quad (12)$$

When the ratio of rational activity coefficients ($f_a^{Z_b}/f_b^{Z_a}$) is unity, K_{eq} is equivalent to the Vanselow selectivity coeffi-

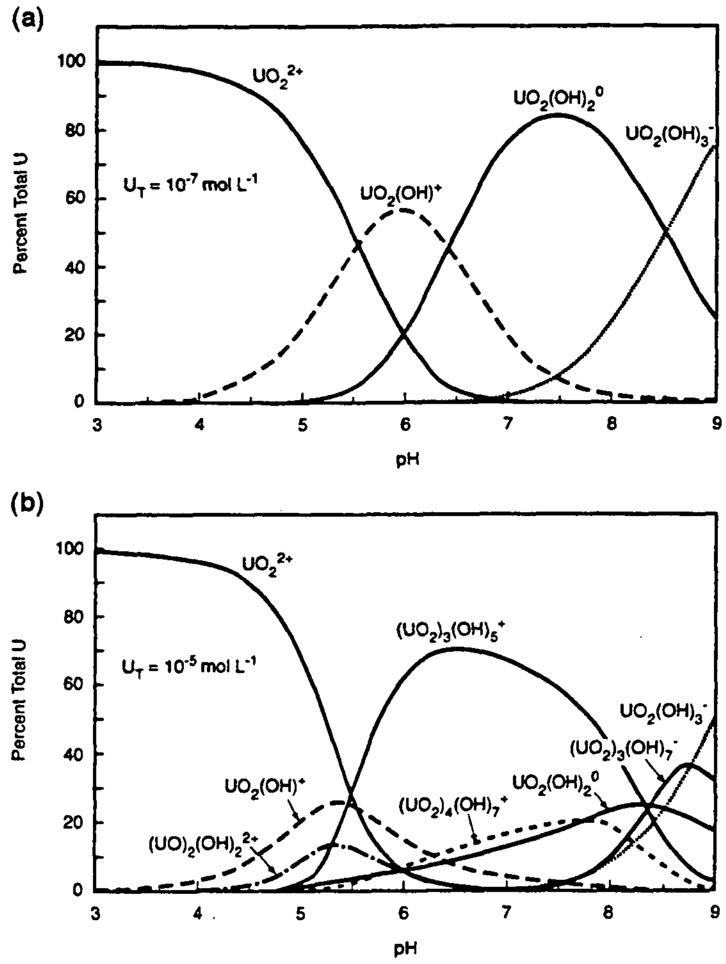

FIG. 4. Computed speciation of UO_2^{2+} as a function of pH at $I = 0.1$ mol L^{-1} a) at 10^{-7} mol L^{-1} $UO_{2(aq)}^{2+}$ and b) at 10^{-5} mol L^{-1} $UO_{2(aq)}^{2+}$. Constants are from Table 4.

cient, K_v. As an initial approximation, all exchange reactions between UO_2^{2+}, Al^{3+}, and their hydrolyzed species with NaX were assumed to be ideal (i.e., $f_i = 1$) and were assigned $K_{eq} = K_v = 1$. The half-reaction constants for these reactions were computed at each data point using Eqn. 10 (Table 2), and with the approximation that for the Na-saturated system,

$$Q = [X^-]_T + [AlO^- -Na^+] + [SiO^- -Na^+], \quad (13)$$

where the species $AlO^- -Na^+$ and $SiO^- -Na^+$ represent the variable charge component of the CEC as discussed previously. Ca^{2+} was assigned a slight preference over Na^+ ($K_v \geq 1$) for fixed charge sites on the basis of experimental work by Fletcher and Sposito (1989) on SWy-1 montmorillonite.

The reactivities of the edge hydroxyl sites were specified by acidity and ion-pair formation constants describing charge development and a set of constants describing the surface complexation of different species of UO_2^{2+}. Aluminol sites were represented by acidity and ion-pair formation constants for α-$Al(OH)_{3(s)}$ (Table 2; McKinley et al., 1996). Silanol sites were represented by analogous constants for α-$SiO_{2(s)}$ (Table 2; Zachara and Smith, 1994). Capacitances and surface areas were fixed as noted in Table 3. Surface complexation constants for UO_2^{2+} by aluminol and silanol sites were computed from UO_2^{2+} adsorption data on α-$Al(OH)_3(s)$ and α-$SiO_2(s)$ (Fig. 5).

The hydrolysis of UO_2^{2+} at low concentrations in noncomplexing media is not completely defined. Most experimental work on the hydrolysis of UO_2^{2+} has been performed at pH < 5 and at UO_2^{2+} concentrations approaching saturation with hydroxide solids (Grenthe, 1992; Baes and Mesmer, 1976). As a result, there are uncertainties associated with the monomeric hydrolysis constants for the species $UO_2(OH)_2^0$ and $UO_2(OH)_3^-$, and with the polymeric hydrolysis constants for the species $(UO_2)_3(OH)_7^-$ and $(UO_2)_4(OH)_7^+$ (Table 4). There has been recent work which provides improved values for the formation constants of the $UO_2(OH)_2^0$ species (Table 4; Torrero et al., 1994; Silva, 1992) and for $UO_2(OH)_3^-$ and $(UO_2)_3(OH)_7^-$ (Table 4; Sandino and Bruno, 1992). The NEA compilation of recommended thermodynamic values for U speciation (Grenthe, 1992), has been revised accordingly (Grenthe et al., 1995). Reducing the formation constant of the $UO_2(OH)_2^0$ species below that reported by Grenthe (1992) results in the computed prevalence of the $(UO_2)_3(OH)_5^+$ species over $UO_2(OH)_2^0$ at 10^{-5} mol L^{-1} $[U]_T$ (Fig. 4b). Over the $[U]_T$ range in this study, the UO_2^{2+} speciation between pH 6 and

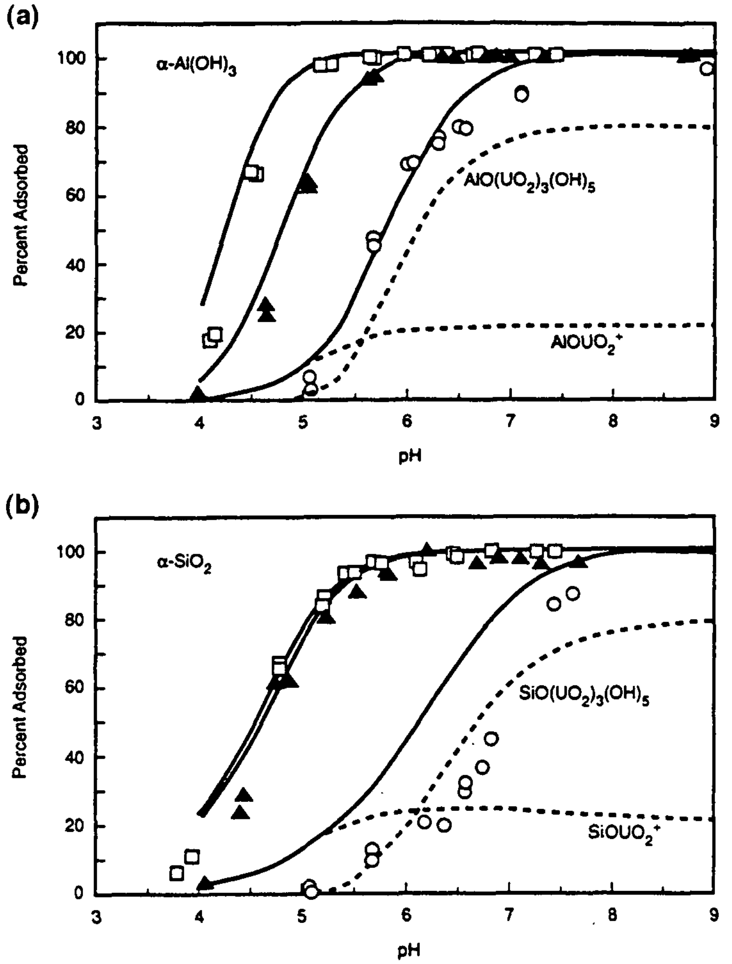

FIG. 5. Percent adsorption of 8.5×10^{-6} mol L^{-1} $UO_{2(aq)}^{2+}$ on gibbsite, α-Al(OH)$_3$ and silica, α-SiO$_2$ in NaClO$_4$ background electrolyte. Data and model are from McKinley et al. (1996). a) □ 5.59 g L^{-1}, I = 0.001 mol L^{-1}; ▲ 5.74 g L^{-1}, I = 0.1 mol L^{-1}; ○ 0.56 g L^{-1}, I = 0.1 mol L^{-1} b) □ 0.15 g L^{-1}, I = 0.001 mol L^{-1}; ▲ 0.13 g L^{-1}, I = 0.1 mol L^{-1}; ○ 0.013 g L^{-1}, I = 0.1 mol L^{-1}. Surface complex species are illustrated with dashed lines for the low solids, high ionic strength data sets (circles).

8 shifts from one dominated by polymeric hydrolysis products to one dominated by monomeric hydrolysis products (Fig. 4a,b).

Following Sandino and Bruno (1992) and McKinley et al. (1996), an aqueous speciation scheme consisting of UO_2^{2+}, $UO_2(OH)^+$, $UO_2(OH)_3^-$, $(UO_2)_2(OH)_2^{2+}$, and $(UO_2)_3(OH)_5^+$ was adopted for all subsequent model calculations (Table 2). This speciation scheme includes all of the hydrolysis products computed to contribute at least 10% at the initial experimental $[U]_T$ with the exception of the $UO_2(OH)_2^0$, $(UO_2)_3OH)_7^-$, and $(UO_2)_4(OH)_7^+$ species. Above pH 6, adsorption decreases $[U]_T$ by ≥2 orders of magnitude; therefore, the $(UO_2)_3(OH)_7^-$ and $(UO_2)_4(OH)_7^+$ species are unlikely to be important. The solubility data of Silva (1992) indicate a lower value for the formation constant of the $UO_2(OH)_2^0$ species than his model computations predict; and, only a revised upper limit was suggested in the revised thermodynamic compilation (Grenthe et al., 1995). The contribution of the $UO_2(OH)_2^0$ species is likely overstated using this upper limit as the stability constant. With this set of aqueous hydrolysis constants, the adsorption of UO_2^{2+} on α-Al(OH)$_3$(s) and α-SiO$_2$(s) was well-described over a wide range of solution conditions using two surface complexes (SO-UO_2^+ and SO$^-$–$(UO_2)_3(OH)_5$; Fig. 5a,b].

The ensemble of surface complex species used here and by McKinley et al. (1996) are not unique, and are sensitive to the particular suite of aqueous species used. The adsorption of UO_2^{2+} on α-Al(OH)$_3$(s) was equally well described by including the $UO_2(OH)_2^0$ species. However, the formation constants of the $UO_2(OH)_2^0$ and $UO_2(OH)_3^-$ species had to be adjusted to −12.5 and −22.0, respectively, to achieve good fit, and the surface complex species AlO$(UO_2)(OH)^0$ was predicted to dominate (data not shown).

Our surface speciation scheme for both alumina and silica [SO-UO_2^+; SO-$(UO_2)_3(OH)_5$] was based on goodness of fit to the macroscopic sorption data rather than spectroscopic evidence. This surface speciation scheme is similar to that used by Hsi and Langmuir (1985) on ferrihydrite [SO-UO_2OH; SO-$(UO_2)_3(OH)_5$]. Waite et al. (1994) argued against the formation of a SO-$(UO_2)_3(OH)_5$ complex, but the data upon which their argument was based (their Fig.

Table 2. Equilibrium Constants Used for Surface and Solution Reactions

Reactions	log K_f
Edge-Site Reactions	
$SiOH = SiO^- + H^+$	-6.95 [a]
$SiOH + Na^+ = SiO^-{-}Na^+ + H^+$	-6.6 [a]
$SiOH + UO_2^{2+} = SiOUO_2^+ + H^+$	0.146 [b]
$SiOH + 3UO_2^{2+} + 5H_2O = SiO(UO_2)_3(OH)_5 + 6H^+$	-16.8 [b]
$AlOH + H^+ = AlOH_2^+$	7.6 [b]
$AlOH = AlO^- + H^+$	-10.6 [b]
$AlOH + Na^+ = AlO^-{-}Na^+ + H^+$	-7.3 [b]
$AlOH + H^+ + ClO_4^- = AlOH_2^+{-}ClO_4^-$	10.7 [b]
$AlOH + UO_2^{2+} = AlOUO_2^+ + H^+$	2.47 [c]
$AlOH + 3UO_2^{2+} + 5H_2O = AlO(UO_2)_3(OH)_5 + 6H^+$	-17.7 [c]
Ion-Exchange Reactions	
$Na^+ + X^- = NaX$	10.0 [c,d]
$H^+ + X^- = HX$	10.1 [c,d]
$Ca^{2+} + 2X^- = CaX_2$	23.4 [c,d]
$UO_2^{2+} + 2X^- = UO_2X_2$	23.2 [c,d]
$UO_2^{2+} + H_2O + X^- = UO_2(OH)X + H^+$	4.8 [c,d]
$Al^{3+} + 3X^- = AlX_3$	36.5 [c,d]
$Al^{3+} + H_2O + 2X^- = Al(OH)X_2 + H^+$	18.2 [c,d]
$Al^{3+} + 2H_2O + X^- = Al(OH)_2X + 2H^+$	-0.10 [c,d]
Aqueous Speciation	
$UO_2^{2+} + H_2O = UO_2(OH)^+ + H^+$	-5.2 [e]
$UO_2^{2+} + 3H_2O = UO_2(OH)_3^- + 3H^+$	-21.2 [e]
$2UO_2^{2+} + 2H_2O = (UO_2)_2(OH)_2^{2+} + 2H^+$	-5.62 [e]
$3UO_2^{2+} + 5H_2O = (UO_2)_3(OH)_5^+ + 5H^+$	-15.55 [e]
$Al^{3+} + H_2O = Al(OH)^{2+} + H^+$	-4.99 [f]
$Al^{3+} + 2H_2O = Al(OH)_2^+ + 2H^+$	-10.1 [f]
$Al^{3+} + 3H_2O = Al(OH)_{3(aq)} + 3H^+$	-16.0 [f]
$Al^{3+} + 4H_2O = Al(OH)_4^- + 4H^+$	-23.0 [f]
$H_4SiO_4 = H_3SiO_4^- + H^+$	-9.71 [g]

[a] Zachara and Smith, 1994

[b] McKinley et al., 1996

[c] this study

[d] half-reaction constants for a 1.5 g kg^{-1} suspension, assuming $Q = [X^-]_T$, calculated with eq. 10 according to the convention of Fletcher and Sposito, 1989.

[e] Table 4

[f] Nordstrom and May, 1989

[g] Lindsay, 1979

5) does not seem conclusive. These authors also found that XAS/EXAFS spectra of UO_2 sorbed to ferrihydrite were consistent with the formation of a bidentate surface complex, and a (FeO_2)-UO_2 complex on hypothetical weak and strong sites was used as their basis for surface complexation modeling. The degrees of freedom in the model calculations of

Table 3. Triple-Layer Model Parameters

	Surface Area [c] $m^2\,g^{-1}$	Site Density [d] sites nm^{-2}	Inner Capacitance F m^{-2}	Outer Capacitance F m^{-2}
α-$Al(OH)_3$ [a]	11	4.0	0.80	0.2
α-SiO_2 [b]	183	4.5	1.30	0.2
Kenoma [c]	99		1.05	0.2

[a] McKinley et al., 1996

[b] original parameters from Riese (1982); surface area of material in original study was 4.15 $m^2\,g^{-1}$

[c] composite model, this study

[d] used for fitting adsorption constants for UO_2^{2+} on the two single phase sorbents, α-$Al(OH)_3$ and α-SiO_2

Table 4. Sources of Proposed UO_2^{2+} Hydrolysis Constants and Uncertainties at 25° C and I = 0

	log K° ± 2σ
$UO_2^{2+} + H_2O = UO_2(OH)^+ + H^+$	-5.2 ± 0.3 [a]
$UO_2^{2+} + 2H_2O = UO_2(OH)_2^0 + 2H^+$	≤ -11.5 [b]
$UO_2^{2+} + 3H_2O = UO_2(OH)_3^- + 3H^+$	-20.0 ± 0.5 [c]
$2UO_2^{2+} + 2H_2O = (UO_2)_2(OH)_2^{2+} + 2H^+$	-5.62 ± 0.04 [a]
$3UO_2^{2+} + 5H_2O = (UO_2)_3(OH)_5^+ + 5H^+$	-15.55 ± 0.12 [a]
$3UO_2^{2+} + 7H_2O = (UO_2)_3(OH)_7^- + 7H^+$	-32.7 ± 0.8 [c]
$4UO_2^{2+} + 7H_2O = (UO_2)_4(OH)_7^+ + 7H^+$	-22 ± 1 [a]

[a] Grenthe (1992)
[b] Silva (1992)
[c] Sandino and Bruno (1992)

Waite et al. (1994), two sites and one surface complex species, and this study, one site and two surface species, were the same and both yielded comparable fits to the data. Spectroscopic information is unavailable for UO_2 on silica or alumina upon which to anchor surface complexation modeling, i.e., surface bonding denticity and plausibility of the 3.5 species as a surface complex.

4.2. Model Calibration

The surface-complexation model was calibrated by calculating site concentrations for X^-, AlOH, and SiOH on the subsurface smectite that were consistent with measured adsorbed cation and proton charge data. Optimization consisted of minimizing the weighted residuals of the material balance equation:

$$Y_j = \Sigma b_{ij} C_i - T_j, \qquad (14)$$

where Y_j is the residual of the jth component, $\Sigma b_{ij} C_i$ is the calculated concentration of component j from the concentration of all i species containing component j (C_i), b_{ij} is the stoichiometry coefficient of j in species i, and T_j is the measured total concentration of component j.

Site concentrations are often calculated from potentiometric titration data. However, because dissolution complicated the proton adsorption data, site concentrations were fit from Na^+ material-balance data obtained through measurement of adsorbed cation charge. The fitted objective function was the CEC (Eqn. 3, Fig. 2a). To simplify the equilibrium problem, it was assumed that the clay was Na^+ saturated with no exchangeable Al^{3+}. However, the presence of fixed-charge sites occupied by Al^{3+} in our electrolyte adsorption experiment (Fig. 2a) was explicitly considered through the CEC:

$$[Na^+]_T = [Na^+]_X + (CEC \cdot Y), \qquad (15)$$

where $[Na^+]_X$ is the free aqueous concentration (mol L^{-1}) determined by IC, CEC is defined by Eqn. 3, and Y is the clay mass (kg L^{-1}). The summation in Eqn. 14 was defined by Eqn. 4. That is,

$$\Sigma b_{ij} C_i = [NaX] + [SiO^- \text{-} Na^+] + [SiO^- - Na^+] + [AlO^- \text{-} Na^+] + [AlO^- - Na]. \qquad (16)$$

The concentration of Na^+ adsorbed on fixed charge sites (NaX) was computed conventionally within FITEQL from its half reaction (Eqn. 12) and appropriately fixed constant. The remaining species represent the concentration of Na^+ adsorbed on variable charge sites. The species SiO^--Na^+ and AlO^--Na^+ represent specifically bound, outersphere surface complexes defined by the TLM, and were computed conventionally within FITEQL from the ion-pair formation constants of the analog components. The species SiO^-–Na^+ and AlO^-–Na^+ represent nonspecifically bound Na^+ in the diffuse layer, and were computed by assuming that Na^+ associates as a counterion with each SiO^- and AlO^- species. The variable charge component of the CEC was, therefore, assumed to equal the combined concentrations of SiO^- and AlO^- that were computed from the acidity and ion-pair formation constants of the analog components. The SiO^- and AlO^- species were included in the Na^+ material balance equation by appropriate stoichiometry specifications within the material balance matrix.

The multiple-site model readily converged on the CEC data and provided an excellent description of its trend with pH (Fig. 2b). Given the analogue phase assumption, the model indicated that SiO^- was the principal source of pH-variable charge; it influenced the CEC through counterion binding. Although the species AlO^--Na^+ and AlO^- did not contribute significantly to the calculated CEC, the aluminol site affected the fitted parameters through an electrostatic influence on SiOH ionization. Within FITEQL, the electrostatic parameter is treated as a component, with a single material-balance equation spanning all hydroxyl sites. Thus, sites with differing acid-base properties exhibit an interactive effect on the ionization of each other, analogous to the smectite edge. Consequently, the removal of the aluminol site resulted in poorer fits to the CEC (not illustrated).

The sum of the hydroxyl site concentrations computed by the model (4.25×10^{-4} mol g^{-1}) were 50% lower than the value measured by ^3H exchange (8.61×10^{-4} mol g^{-1}) and 263% greater than the value calculated from mean particle

Table 5. Estimated and Optimized Site Concentrations in Kenoma Isolate

	Mean Particle Diameter [a,b]	^{3}H Exchange [b,c]	Accessible Structural Surface Charge [d]	Optimized Values [e]
	$\times 10^{-2}$ mol kg^{-1}			
X^-	-	-	34.8	39.7
SiOH	5.72	42.1	-	20.5
AlOH	5.98	44.0	-	22.0
$[SOH]_T$	11.70	86.1	-	42.5

[a] mean particle diameter by transmission electron microscopy (Zachara and Smith, 1994)
[b] fraction of SiOH and AlOH sites calculated from edge site densities reported by White and Zelazny (1988)
[c] tritium exchange from this study based on the procedure of Yates (1975)
[d] accessible structural surface charge from this study based on the procedure of Anderson and Sposito (1991)
[e] this study

diameter (1.17×10^{-4} mol g^{-1}; Table 5); however, these site concentrations adequately predicted the independently determined proton adsorption data (Fig. 1b). The total concentration of fixed-charge sites, $[X^-]_T$, computed by the model (Table 5), compared favorably to the concentration measured directly using the procedure of Anderson and Sposito (1991). Also, the computed concentration of $SiO^- - Na^+$ at pH 6 (0.085 mol kg^{-1}; Fig. 2b) was comparable to the experimentally measured value of $[SO^-]$ (0.15 mol kg^{-1}, Table 1). The ratio of aluminol to silanol sites calculated from our model, 1.07, compared well with the value of 1.04 reported by White and Zelazny (1988) for the edge of beidellite. We considered this level of agreement between computation and experimental measurement good, given ambiguities in the measurements and the assumptions of the model.

4.3. Calculations of Uranyl Adsorption

In our first application of the multiple-site model to describe UO_2^{2+} adsorption to the subsurface smectite, we used the concentrations of X^-, SiOH, and AlOH sites derived from Fig. 2b (Table 5), surface equilibrium constants for AlOH and SiOH analogue phases (Table 2), and unit ion-exchange constants ($K_v = 1.0$) for UO_2^{2+}, Al^{3+}, and their hydrolyzed species. The ion-exchange process was therefore ternary, either Na^+-Al^{3+}-UO_2^{2+} or Ca^{2+}-Al^{3+}-UO_2^{2+}. These total concentrations and equilibrium constants, along with serial data for $[Al]_T$ from Fig. 1a, were input to FITEQL, which was used to predict UO_2^{2+} adsorption. These calculations significantly overpredicted the amount of adsorption (data not shown). The overprediction was a consequence of the magnitude of UO_2^{2+} binding to the aluminol sites on the smectite edge.

The adsorption data could be described well if the binding constants for UO_2^{2+} and $(UO_2)_3(OH)_5^+$ with edge AlOH were uniformly reduced by 2.03 log units below gibbsite (Fig. 6, Table 2). In Na electrolyte, the computed surface speciation of uranyl was dominated by the ion-exchange complex (UO_2X_2) at low pH and ionic strength (Fig. 6a), and by edge coordination complexes at higher ionic strength and pH (Fig. 6b). The ionic strength and electrolyte cation effects were adequately described as a consequence of ion exchange with the assumption of unit K_v's (Fig. 3), although UO_2^{2+} sorption was over and under predicted below pH 5.5 at the lowest and highest ionic strengths, respectively. Even with the reduction in UO_2^{2+} binding constants for the aluminol sites, surface complexes with AlOH sites were computed to dominate uranyl binding to the smectite edge (Fig. 6). Similarly, Cu^{2+} adsorption to the smectite edge was postulated to occur via coordination to aluminol, rather than silanol sites (Stadler and Schindler, 1993).

The hypothesis of $K_v = K_{eq} = 1$ for all exchange reactions, combined with the other model parameters, yielded calculated concentrations of exchangeable Al^{3+} that agreed precisely with the experimental values obtained by La^{3+} extraction (Fig. 2a). The computations suggested that exchangeable Al^{3+} was dominated by the AlX_3 complex, with an insignificant contribution from hydrolyzed species [i.e., $AlOHX_2$, $Al(OH)_2X$]. The concentration of fixed charge sites consumed by Al^{3+}, however, was not large enough to significantly impact UO_2^{2+} exchange above pH 4.

4.4. Gibbsite as an Analogue Phase

The need to reduce the UO_2^{2+} binding constants to the aluminol sites to achieve good model fit requires comment, since the combination of AlOH site concentration (Table 5) and the gibbsite proton association/dissociation constants (Table 2) appeared to yield an adequate description of the proton adsorption data (Fig. 2). Furthermore, gibbsite has been used by others as a potential model phase for the smectite edge (McKinley et al., 1996), and a critique of its applicability is warranted. Three explanations are plausible: (1) edge site concentrations have been overestimated, (2) gibbsite is not a relevant analogue phase, and (3) competitive sorption reactions with Al^{3+} or H_4SiO_4 on the aluminol site have decreased their apparent selectivity.

4.4.1. Site concentration

Edge-site concentrations of aluminol sites were estimated from the Na-material balance data (Fig. 2) assuming the surface acidity behavior of gibbsite. The Na-material balance data is not the most sensitive dataset from which to estimate

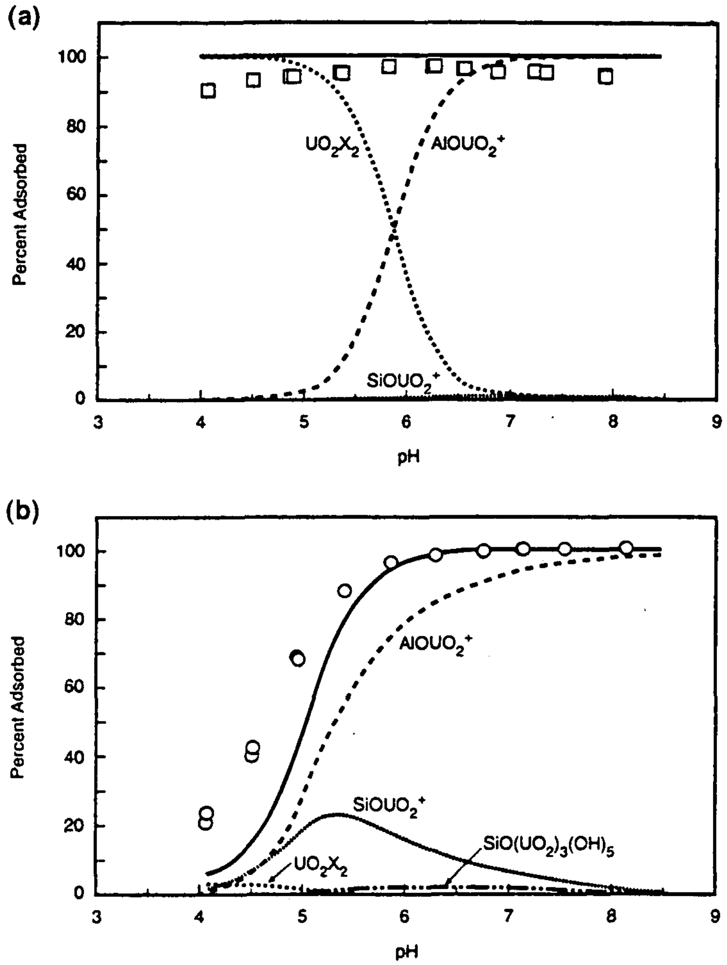

FIG. 6. Computed UO_2^{2+} surface complex speciation for the DCB/H_2O_2 treated Kenoma smectite in (a) 0.001 mol L^{-1} $NaClO_4$ electrolyte and (b) 0.1 mol L^{-1} $NaClO_4$ electrolyte. Surface complex species are illustrated with dashed lines, and model totals are illustrated with solid lines.

SOH concentrations because it is dominated by the ion exchange component, but it was used to achieve an internally consistent set of concentrations for the surface components. When normalized to the reported $N_{2(g)}$ surface areas, our total hydroxyl site concentration, 4.29×10^{-6} mol m^{-2}, was consistent with that reported for SWy-1 (4.45×10^{-6} mol m^{-2}; Stadler and Schindler, 1993); however, our total site concentration was 4.8 times higher than that reported for bentonite (8.88×10^{-7} mol m^{-2}; Wanner et al., 1994). Our estimated concentration of aluminol sites, 2.2×10^{-6} mol m^{-2}, also compared favorably with that reported for SWy-1 (2.79×10^{-6} mol m^{-2}; Stadler and Schindler, 1993). We offer these comparisons only to show that our site concentrations are not unreasonable, given those reported by others. It is noted without comment that our clay was prepared and treated differently from that of Stadler and Schindler (1993), who began their potentiometric titrations under generally acidic conditions.

While our edge-site concentrations, and particularly those of the aluminol sites, may be relevant for the proton, structural and coordination chemical aspects of the edge may limit UO_2^{2+} adsorption to a subset of these sites. Further comment is not possible without the careful measurement (in the absence of surface precipitation of UO_2^{2+} solid phases) of the surface concentration of UO_2^{2+} at edge site saturation.

4.4.2. *Structural considerations*

That gibbsite does not function as a quantitative model for UO_2^{2+} adsorption on the exposed edge of the octahedrally coordinated alumina layer (OCAL) is not totally unexpected. While gibbsite and the OCAL exhibit similarities in structure, they differ in two key attributes. First, formal cation charge in the OCAL is satisfied by a combination of doubly coordinated hydroxyl ions and coshared oxygens with the Si(IV) tetrahedral layer; in gibbsite formal charge on Al(III) is satisfied by doubly coordinated hydroxyls only. Second, isomorphic substitutions of divalent cations occur in the OCAL that lead to a net charge deficit, while the bulk gibbsite structure is electrically neutral. As a result of these factors, the structure and hydroxyl site distribution of the

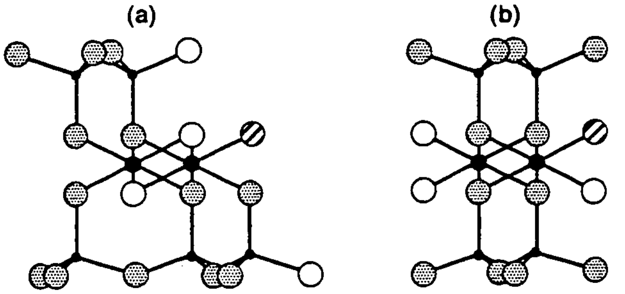

FIG. 7. Profile of two 2:1 phyllosilicate edge faces adapted from White and Zelazny (1988). The edge face is on the right-hand side in each illustration with the phyllosilicate layer extending to the left. The A-chain (a) runs parallel to the [110] crystallographic direction and borders the {110} edge face. The B-chain (b) runs parallel to the [100] crystallographic direction and borders the {010} edge face. Shaded circles denote oxygens, open circles are hydroxyls, striped circles are water molecules, and small filled circles are Al atoms. Figure and caption from Bleam et al. (1993).

OCAL edge may be different from the edge of gibbsite. Such differences have proved difficult to isolate from macroscopic measurements such as proton adsorption because of the other competing reactions that occur.

Structural models (A and B chain) have been developed for the 2:1 phyllosilicate edge (White and Zelazny, 1988; Bleam et al., 1993). The A and B chain models run parallel to the [110] and [100] directions in phyllosilicates (Fig. 7), and represent potential edge structures exposed to solution in aqueous smectite suspensions. Hydroxyls with single and double coordination to Al(III) are expected, as well as Lewis acid sites (e.g., Al-OH$_2$) (Fig. 7). Of these, the singly coordinated and Lewis acid sites are most reactive (Sposito, 1984; Hiemstra et al., 1989a,b). The relative distribution of the A and B chain structures is dependent on the smectite crystallite morphology, but on average the ratio of single to doubly coordinated hydroxyls within these models is 3:2. The proposed edge structure of gibbsite is partially analogous to the aluminous core of the B chain model (Hiemstra et al., 1987), and Hiemstra et al. (1989b) suggested that the ratio of single to doubly coordinated hydroxyls on the gibbsite edge was 2:1. It appears, therefore, that the site density and overall concentration of reactive Al-bound hydroxyls on the smectite edge may be comparable to that on gibbsite.

The singly coordinated hydroxyls and the Lewis acid sites on the OCAL edge, however, differ from comparable ones on gibbsite in that they are bound to Al(III) ions that coshare three or four oxygens with Si(IV) in their coordination sphere (Fig. 7.). Such coordination to the Si(IV) cation may decrease the coordinative strength of the Al-O$^-$ ligand for metal ion sorbates such as UO$_2^{2+}$. Additionally, the smectite edge may be structurally less conducive to surface complex formation than gibbsite. Using X-ray absorption spectroscopy, Waite et al. (1994) observed that UO$_2^{2+}$ appeared to form a bidentate, mononuclear surface complex on ferrihydrite, and O'Day et al. (1994) suggested that Co^{2+} formed a bidentate, multinuclear complex with AlOH and adjacent Al-O-Si sites on kaolinite. We may speculate that on the smectite edge, high energy aluminol sites conducive to bidentate, mononuclear complex formation are in short supply (i.e., Fig. 7b) while the multinuclear complexes (if they exist) are of lower stability than the dominant surface complex types on gibbsite.

4.4.3. *Competitive interactions*

The Kenoma smectite was equilibrated at pH 4 for approximately 12 h at the initiation of the uranyl sorption experiments. Under these conditions, significant Al^{3+} was solubilized by proton promoted dissolution of the clay isolate (c.a., 10^{-3} mol L^{-1}; Fig. 1). Because UO$_2^{2+}$ sorption was determined using a continuous batch titration (in contrast to our electrolyte and proton adsorption experiments), this solubilized Al^{3+} remained in the clay suspension and may have impacted UO$_2^{2+}$ sorption as the suspension pH was incrementally raised to its final value. While the effects of La^{3+} exchangeable Al^{3+} were explicitly and quantitatively addressed in our treatment of the uranyl ion exchange equilibria and the material balance of fixed charge sites (X^-), no comparable consideration was given to the potential sorption of Al^{3+} to the smectite edge sites.

Aluminum, in fact, is strongly coordinated to the edge sites of smectite, exhibiting a pH adsorption edge on SWy-1 at approximately pH 4.75 (with SWy-1 at approximately 2.0 g L^{-1}; Charlet et al., 1993). Qualitative comparisons of experimental data with SWy-1 at higher ionic strengths (e.g., 0.1 mol L^{-1}; Charlet et al., 1993; McKinley et al., 1996), indicate that both Al^{3+} and UO$_2^{2+}$ are sorbed with comparable, high affinity to edge sites. The apparent decrease in our La^{3+} extractable Al^{3+} with increasing pH may be explained as a shift in the distribution of Al^{3+} surface complexes from those dominated by weak, outer-sphere, ion-exchange complexes at lower pH to strong, inner-sphere complexes on edge sites at higher pH that are not La^{3+} exchangeable. Such inner-sphere edge complexes of Al^{3+} may have suppressed UO$_2^{2+}$ complexation to these sites by competitive mass action and site blockage. Indeed, the total concentration of Al^{3+} solubilized at pH 4, 10^{-3} mol L^{-1}, exceeded the computed concentration of edge sites present in the Kenoma smectite sorbent suspension, 6.4 × 10^{-4} mol L^{-1}, indicating that it was present in sufficient concentration to impact the material balance of edge sites.

An analogous, although less compelling argument, may be made for the impacts of dissolved silica (concentrations in Fig. 1). Silica adsorbs to Al, Fe, and Mn oxides (Goldberg, 1985; Zachara et al., 1987; Goldberg and Glaubig, 1988; Balistrieri and Chao, 1990), with stronger sorption noted on oxides with high pH$_{ZNPC}$. Dissolved silicic acid released by the clay isolate may have formed surface complexes with edge aluminol sites. While the effects of competition between either Al^{3+} or H$_4$SiO$_4$ with UO$_2^{2+}$ for edge sites are indeterminate from our data, the result of such competition would be to reduce the apparent affinity of the aluminol sites for UO$_2^{2+}$, which agrees with experimental observation.

5. CONCLUSIONS

Uranyl sorption to the subsurface smectite showed contributions from ion exchange and "oxide-like" surface-complexation reactions whose relative effects varied with pH, ionic strength, and the electrolyte cation. At the highest Na electrolyte concentration (0.1 mol L^{-1}) and both Ca electrolyte concentrations (0.05 and 0.05 mol L^{-1}), ion exchange was suppressed and uranyl sorption exhibited "oxide-like" characteristics. Because of these similarities in chemical behavior, a multisite surface-complexation/aqueous-speciation model developed for SWy-1 (McKinley et al., 1996) could be applied to the natural smectite with minimal modification. Unlike SWy-1, however, the subsurface smectite released greater concentrations of Al^{3+} that required explicit consideration for measuring surface charge. Dissolution reactions may be more important in subsurface materials, where minor mineralogic components or poorly crystalline phases contribute to high solubilities of both Al^{3+} and H_4SiO_4 under certain pH conditions. The chemistry of Al^{3+} was especially important between pH 4 and 6. Aluminum dissolution and adsorption caused a stronger apparent pH dependency for CEC as determined by Na^+ adsorption then actually existed.

A surface-charge model was developed for the natural smectite based on measurements of Na^+ adsorption and exchangeable Al^{3+}. This model provided good replications of the proton adsorption data for the clay, which were complicated by the effects of dissolution. Good qualitative agreement between experimental measurements of structural (X^-) and ionized edge charge (SO^-) with independent predictions by the model allowed confidence in its conceptual validity.

The surface-charge model could not be directly applied, using relevant surface-reaction constants for analogue phases, to predict UO_2^{2+} binding to the subsurface smectite. The combination of AlOH site concentrations derived from the electrolyte and proton-binding measurements ($[AlOH]_T$) and the log K for the $AlOUO_2^{2+}$ inner-sphere surface complex on gibbsite (log K_{AlOUO_2}) led to overpredictions of UO_2^{2+} adsorption.

The UO_2^{2+} sorption could only be simulated with a common set of reactions and constants by reducing the effective product of $[AlOH]_T \times K_{AlOUO_2}$. This reduction was accomplished by reducing log K_{AlOUO_2}. The fact that all of the UO_2^{2+} sorption data could be described by adjustment of one parameter, i.e., log K_{AlOUO_2}, suggested that our model contained surface chemical equilibria that were consistent with this complex dataset. We suggest, however, that the affinity of edge AlOH for cationic metal sorbates such as UO_2^{2+} may be significantly below that of comparable sites on gibbsite as a result of the different structural environment of the smectite edge and coordination chemical effects arising from the sharing of oxygens with the adjacent silica layer. Alternatively, $Al^{3+}_{(aq)}$ and $H_4SiO_{4(aq)}$ released by the smectitic isolate may have competed with UO_2^{2+} for edge sites, reducing the apparent affinity of aluminol sites for UO_2^{2+}. Our experimental data did not allow resolution of these contrasting hypotheses.

Acknowledgments—This research was supported by the Subsurface Science Program, Office of Health and Environmental Research, U.S. Department of Energy (DOE). It is a Co-Contaminant Chemistry contribution. The authors thank Sonia Enloe for the text processing and Laurel Grove for editing. Pacific Northwest Laboratory is operated for DOE by Battelle Memorial Institute under Contract DE-AC06-76RLO 1830. The authors thank Dr. Sharon Anderson for her helpful comments on the manuscript and an anonymous reviewer who identified to us recently improved values for U hydrolysis.

Editorial handling: G. Sposito

REFERENCES

Anderson S. J. and Sposito G. (1991) Cesium-adsorption method for measuring accessible structural surface charge. *Soil Sci. Soc. Amer. J.* **55**, 1569–1576.

Babcock K. L. and Schultz R. K. (1970) Isotopic and conventional determination of exchangeable sodium percentage of soil in relation to plant growth. *Soil Sci.* **109**, 19–22.

Baes C. F. and Mesmer R. E. (1976) *The Hydrolysis of Cations.* Wiley.

Balistrieri L. S. and Chao T. T. (1990) Adsorption of selenium by amorphous iron oxyhydroxide and manganese dioxide. *Geochim. Cosmochim. Acta* **54**, 739–751.

Bleam W. F., Welhouse G. J., and Janowiak M. A. (1993) The surface coulomb energy and proton coulomb potentials of pyrophyllite {010}, {110}, {100}, and {130} edges. *Clays Clay Mineral.* **41**, 305–316.

Borchardt G. (1989) Smectites. In *Minerals in Soil Environments* 2nd ed. (ed. J. B. Dixon and S. B. Weed); *Soil Science Society of America Book Ser. No. 1*, pp. 675–728.

Charlet L., Schindler P. W., Spadini L., Furrer G., and Zysset M. (1993) Cation adsorption on oxides and clays: The aluminum case. *Aquatic Sci.* **55**, 291–303.

Chihacek L. J. and Bremner J. M. (1979) A simplified ethylene glycol monoethyl ether procedure for assessment of soil surface area. *Soil Sci. Soc. Amer. J.* **434**, 821–822.

Chisholm-Brause C., Conradson S. D., Buscher C. T., Eller P. G., and Morris D. E. (1994) Speciation of uranyl sorbed at multiple binding sites on montmorillonite. *Geochim. Cosmochim. Acta* **58**, 3625–3631.

Davis J. A. and Kent D. B. (1990) Surface complexation modeling in aqueous geochemistry. In *Mineral-Water Interface Geochemistry* (ed. A. White and M. Hochella, Jr.); *Rev. Mineral.* **23**, pp. 177–260.

Davis J. A. and Leckie J. O. (1978) Surface ionization and complexation at the oxide/water interface II. Surface properties of amorphous iron oxyhydroxide and adsorption of metal ions. *J. Colloid Interface Sci.* **67**, 90–107.

Davis J. A., James R. O., and Leckie J. O. (1978) Surface ionization and complexation at the oxide/water interface. I. Computation of electrical double layer properties in simple electrolytes. *J. Colloid Interface Sci.* **63**, 480–499.

Dent A. J., Ramsay J. D. F., and Swanton S. W. (1992) An EXAFS study of uranyl ion in solution and sorbed onto silica and montmorillonite clay colloids. *J. Colloid Interface Sci.* **150**, 45–60.

Fiala V. (1988) The significance of the clay minerals in the genesis of hydrothermal uranium deposits. *Tenth Conf. Clay Mineralogy and Petrology, Ostrava*, pp. 255–260.

Fletcher P. and Sposito G. (1989) The chemical modelling of clay/electrolyte interactions for montmorillonite. *Clay Mineral.* **24**, 375–391.

Giblin A. M. (1980) The role of clay adsorption in genesis of uranium ores. *Proc. Intl. Symp. Pine Creek Geosyncline*, pp. 521–529.

Goldberg S. (1985) Chemical modeling of anion competition on goethite using the constant capacitance model. *Soil Sci. Soc. Amer. J.* **49**, 851–856.

Goldberg S. and Glaubig A. (1988) Boron and silicon adsorption on an aluminum oxide. *Soil Sci. Soc. Amer. J.* **52**, 87–91.

Grenthe I. (1992) *Chemical Thermodynamics of Uranium.* North-Holland.

Grenthe I., Puigdomenech I., Sandino M. C., and Rand M. N. (1995) Chemical thermodynamics of uranium. In *Chemical Thermodynamics of Americium* (ed. R. J. Silva et al.). Elsevier.

Harward M. E., Carstea D. D., and Sayegh A. H. (1969). Properties of vermiculites and smectites: Expansion and collapse. *Clays Clay Mineral.* **16**, 437–447.

Hiemstra T., Van Riemsdijk W. H., and Bruggenwert M. G. M. (1987) Proton adsorption mechanism at the gibbsite and aluminum oxide solid/solution interface. *Neth. J. Agric. Sci.* **35**, 281–293.

Hiemstra T., Van Riemsdijk W. H., and Bolt G. H. (1989a) Multisite proton adsorption modeling at the solid/solution interface of (Hydr) oxides: A new approach. I. Model description and evaluation of intrinsic reaction constants. *J. Colloid Interface Sci.* **133**, 91–104.

Hiemstra T., De Wit J. C. M., and Van Riemsdijk W. H. (1989b) Multisite proton adsorption modeling at the solid/solution interface of (Hydr) oxides: A new approach. II. Application to various important (Hydr) oxides. *J. Colloid Interface Sci.* **133**, 105–117.

Hsi D. C. and Langmuir D. (1985) Adsorption of uranyl onto ferric oxyhydroxides: Application of the surface complexation site-binding model. *Geochim. Cosmochim. Acta* **49**, 1931–1941.

Kittrick J. A. and Hope E. W. (1963) A procedure for particle-size separation of soils for X-ray diffraction analysis. *Soil Sci.* **96**, 319–325.

Komadel P., Lear P. R., and Stucki J. W. (1990) Reduction and reoxidation of nontronite: Extent of reduction and reaction rates. *Clays Clay Mineral.* **38**, 203–208.

Lear P. R. and Stucki J. W. (1989) Effect of iron oxidation state on the specific surface area of smectites. *Clays Clay Mineral.* **33**, 539–545.

Lieser K. H., Quandt-Klenk S., and Thybusch B. (1992) Sorption of uranyl ions on hydrous silicon dioxide. *Radiochim. Acta* **57**, 45–50.

Lieser K. H. and Thybusch B. (1988) Sorption of uranyl ions on hydrous titanium dioxide. *Fresenius Z Anal. Chem.* **332**, 351–357.

Lindsay W. (1979) *Chemical Equilibria in Soils.* Wiley.

May H. M., Kinniburgh D. G., Helmke P. A., and Jackson M. L. (1986) Aqueous dissolution, solubility and thermodynamic stabilities of common alumino-silicate clay minerals: Kaolinite and smectites. *Geochim. Cosmochim. Acta* **50**, 1667–1677.

McKinley J. P., Zachara J. M., Smith S. C., and Turner G. D. (1995) The influence of hydrolysis and multiple site-binding reactions on adsorption of U(VI) to montmorillonite. *Clays and Clay Mineral.* **43**, 586–598.

Morris D. E., Chisholm-Brause C. J., Barr M. E., Conradson S. D., and Eller P. G. (1994) Optical spectroscopic studies of the sorption of UO_2^{2+} species on a reference smectite. *Geochim. Cosmochim. Acta* **58**, 3613–3623.

Morrison S. J. and Cahn L. S. (1991) Mineralogical residence of alpha-emitting contamination and implications for mobilization from uranium mill tailings. *J. Contam. Hydrol.* **8**, 1–21.

Nordstrom D. K. and May H. M. (1989) Aqueous equilibrium data for mononuclear aluminum species. In *The Environmental Chemistry of Aluminum* (ed. G. Sposito), pp. 29–55. CRC Press.

O'Day P. A., Parks G. A., and Brown G. E., Jr. (1994) Molecular structure and binding sites of cobalt(II) surface complexes on kaolinite from x-ray absorption spectroscopy. *Clays Clay Mineral.* **42**, 337.

Parker J. C., Zelazny L. W., Sampath S., and Harris W. G. (1979) A critical evaluation of the extension of zero point of charge (ZPC) theory to soil systems. *Soil Sci. Soc. Amer. J.* **43**, 668–674.

Payne T. E. and Waite T. D. (1991) Surface complexation modeling of uranium sorption data obtained by isotopic exchange techniques. *Radiochim. Acta* **52/53**, 487–493.

Riese A. C. (1982) Adsorption of radium and thorium on quartz and kaolinite: A comparison of solution/surface equilibrium models. Ph.D. dissertation, Colorado School of Mines.

Riley R. G., Zachara J. M., and Wobber F. J. (1992) *Chemical Contaminants on DOE Lands and Selection of Contaminant Mixtures for Subsurface Science Research; Report DOE/ER-0547T.* U.S. Department of Energy.

Sandino A. and Bruno J. (1992) The solubility of $(UO_2)_3(PO_4)_2 \cdot 4H_2O(s)$ and the formation of U(VI) phosphate complexes: Their influence in uranium speciation in natural waters. *Geochim. Cosmochim. Acta* **56**, 4135–4145.

Schindler P. W., Liechti P., and Westall J. C. (1987) Adsorption of copper, cadmium, and lead from aqueous solution to the kaolinite/water interface. *Neth. J. Ag. Sci.* **35**, 219–230.

Silva R. J. (1992) Mechanisms for the retardation of uranium (VI) migration. *Mat. Res. Soc. Symp. Proc.* **257**, 323–330.

Sposito G. (1984) *The Surface Chemistry of Soils.* Oxford Univ. Press.

Stadler M. and Schindler P. W. (1993) Modeling of H^+ and Cu^{2+} adsorption on calcium-montmorillonite. *Clays Clay Mineral.* **41**, 288–296.

Thomson B. M., Longmire P. A., and Brookins D. G. (1986) Geochemical constraints on underground disposal of uranium mill tailings. *Applied Geochem.* **1**, 335–343.

Torrero M. E., Casas I., De Pablo J., Sandino M. C. A., and Grambow B. (1994) A comparison between unirradiated $UO_2(s)$ and schoepite solubilities in 1 M NaCl medium. *Radiochim. Acta* **66/67**, 29–35.

Tsunashima A., Brindley G. W., and Bastovanov M. (1981) Adsorption of uranium from solutions by montmorillonite: Compositions and properties of uranyl montmorillonites. *Clays Clay Mineral.* **29**, 10–16.

Waite T. D., Davis J. A., Payne T. E., Waychunas G. A., and Xu N. (1994) Uranium(VI) adsorption to ferrihydrite. Application of a surface complexation model. *Geochim. Cosmochim. Acta* **58**, 5465–5478.

Wanner H., Albinsson Y., Karnland O., Wieland E., Wersin P., and Charlet L. (1994) The acid/base chemistry of montmorillonite. *Radiochim. Acta* **66/67**, 157–162.

Westall J. C. (1982a) *FITEQL. A Computer Program for Determination of Equilibrium Constants form Experimental Data. Version 1.2. Report 82-01.* Department of Chemistry, Oregon State Univ.

Westall J. C. (1982b) *FITEQL. A Computer Program for Determination of Equilibrium Constants from Experimental Data. Version 2.0. Report 82-02.* Department of Chemistry, Oregon State Univ.

Westall J. C., Jones J. D., Turner G. D., and Zachara J. M. (1995) Models for association of metal ions with heterogeneous environmental sorbents. I. Complexation of Co(II) by Leonardite humic acid as a function of pH and $NaClO_4$ concentration. *Environ. Sci. Technol.* **29**, 951–959.

White G. N. and Zelazny L. W. (1988) Analysis and implications of the edge structure of dioctahedral phyllosilicates. *Clays Clay Mineral.* **36**, 141–146.

Williams L. A., Parks G. A., and Crerar D. A. (1985) Silica diagenesis. I. Solubility controls. *J. Sed. Petrol.* **55**, 301–311.

Yates D. E. (1975) The structure of the oxide/aqueous electrolyte interface. Ph.D. dissertation, Univ. Melbourne, Australia.

Zachara J. M. and McKinley J. P. (1993) Influence of hydrolysis on the sorption of metal cations by smectites: Importance of edge coordination reactions. *Aquatic Sci.* **55**, 250–261.

Zachara J. M. and Smith S. C. (1994) Edge complexation reactions of cadmium on specimen and soil-derived smectite. *Soil Sci. Soc. Amer. J.* **58**, 762–769.

Zachara J. M., Smith S. C., McKinley J. P., and Resch C. T. (1993) Cadmium sorption on specimen and soil smectites in Na^+, Ca^{2+}, and Na^+/Ca^{2+} electrolytes. *Soil Sci. Soc. Amer. J.* **57**, 1491–1501.

Zachara J. M., Girvin D. C., Schmidt R. L., and Resch C. T. (1987) Chromate adsorption on amorphous iron oxyhydroxide in the presence of major groundwater ions. *Environ. Sci. Technol.* **21**, 589–594.

SEP 2002
RECEIVED
RECORDS CENTER